# Reconstructing Optical Flow Fields by Motion Inpainting

Benjamin Berkels[1], Claudia Kondermann[2],
Christoph Garbe[2], and Martin Rumpf[1]

[1] Institute for Numerical Simulation, Universität Bonn,
Endenicher Allee 60, 53115 Bonn, Germany
{benjamin.berkels, matrin.rumpf}@ins.uni-bonn.de
WWW home page: http://numod.ins.uni-bonn.de/
[2] IWR,Universität Heidelberg,
Im Neuenheimer Feld 368, 69120 Heidelberg
{Claudia.Kondermann, Christoph.Garbe}@iwr.uni-heidelberg.de
WWW home page: http://hci.iwr.uni-heidelberg.de/

**Abstract.** An edge-sensitive variational approach for the restoration of optical flow fields is presented. Real world optical flow fields are frequently corrupted by noise, reflection artifacts or missing local information. Still, applications may require dense motion fields. In this paper, we pick up image inpainting methodology to restore motion fields, which have been extracted from image sequences based on a statistical hypothesis test on neighboring flow vectors. A motion field inpainting model is presented, which takes into account additional information from the image sequence to improve the reconstruction result. The underlying functional directly combines motion and image information and allows to control the impact of image edges on the motion field reconstruction. In fact, in case of jumps of the motion field, where the jump set coincides with an edge set of the underlying image intensity, an anisotropic TV-type functional acts as a prior in the inpainting model. We compare the resulting image guided motion inpainting algorithm to diffusion and standard TV inpainting methods.

## 1 Introduction

Many methods have been proposed to estimate motion in image sequences. Yet, in difficult situations such as multiple motions, aperture problems or occlusion boundaries optical flow estimates are often incorrect. These incorrect flow patterns can be detected and removed from the flow field e.g. by means of confidence measures [1–3]. But since many applications demand a dense flow field, it would be beneficial to reconstruct a reliable dense vector field based on information from the surrounding flow field. A similar task has been addressed in the field of image reconstruction and is called inpainting, picking up a classical term from the restoration of old and damaged paintings. The digital reconstruction of corrupted images was first proposed by Masnou and Morel [4]. Over the last decade

a wide range of methods has been developed for the inpainting of grayscale or color images. Edge preserving TV inpainting and curvature-driven diffusion inpainting was suggested by Chan and Shen [5, 6]. Transport based methods with a fast marching type inpainting algorithm were proposed by Telea [7] and improved by Bornemann and März [8]. The relation to fluid dynamics was studied by Bertalmio et al. [9] and Chan and Shen [10] investigated texture inpainting. Already in 1993, Mumford et al. [11] proposed to study a variational approach which treats contour lines as elastic curves. In [12], Ballester et al. introduced a variational approach based on the smooth continuation of isophote lines. A variational approach based on level sets and a Perimeter and Willmore energy was presented by Ambrosio and Masnou in [13]. A combination of TV inpainting and wavelet representation was proposed in [14].

The inpainting methodology has been generalized to video sequences with occluding objects by Patwardhan [15]. The reconstruction of motion fields has lately been proposed in the field of video completion. In case of large holes with complicated texture, previously used methods are often not suitable to obtain good results. Instead of reconstructing the frame itself by means of inpainting, the reconstruction of the underlying motion field allows for the subsequent restoration of the corrupted region even in difficult cases. This type of motion field reconstruction called "motion inpainting" was first introduced for video stabilization by Matsushita et al. in [16]. The idea is to continue the central motion field to the edges of the image sequence, where the field is lost due to camera shaking. This is done by a basic interpolation scheme between four neighboring vectors and a fast marching method. Chen et al. [17] refined the approach of Matsushita et al. to obtain a robust motion inpainting approach, which can deal with sudden scene changes by means of Markov Random Field based diffusion and applied it to spatio-temporal error concealment in video coding. In [18], Kondermann et al. proposed to improve motion fields by only computing a few reliable flow vectors and filling in the missing vectors by means of a diffusion based motion inpainting approach.

In general, the variational reconstruction of optical flow fields can be accomplished by straightforward extension of inpainting functionals for images to two dimensional vector fields. However, these methods usually fail in situations where the course of motion discontinuity lines is unclear, e.g. if objects with curved boundary move or junctions occur in overlapping motion. Since image edges often correspond to motion edges the information drawn from the image sequence can be important for the reconstruction, especially in such cases where the damaged vector field does not contain enough information to determine the shape of the motion discontinuity.

In the special case of optical flow extracted from an image sequence, the underlying image sequence itself provides additional information, which can be used to guide the reconstruction process in ambiguous cases. So far, optical flow fields have already been used for the reconstruction of images in video restoration, e.g. in [15]. Here, we use the underlying image data to improve the reconstruction of the optical flow field. The resulting functional is nonlinear and

can be minimized by means of the finite element method. We compare our results to diffusion based and TV inpainting methods.

To prepare the discussion of the proposed new motion field inpainting model, let us briefly review some basic image inpainting methodology. Given an image $u_0 : \Omega \to \mathbb{R}$ and an inpainting domain $D \subset \Omega$, one asks for a restored image intensity $u : \Omega \to \mathbb{R}$, such that $u|_{\Omega \setminus D} = u_0$ and $u|_D$ is a suitable and regular extension of the image intensity $u_0$ outside $D$. The simplest inpainting model is based on the construction of a harmonic function $u$ on $D$ with boundary data $u = u_0$ on $\partial D$. Based on the Dirichlet principle, this model is equivalent to the minimization of the Dirichlet functional $E_{\text{harmon}}[u] = \frac{1}{2}\int_D |\nabla u|^2 \, \mathrm{d}x$ for given boundary data. Due to standard elliptic regularity the resulting intensity function $u$ is smooth – even analytic – inside $D$ but does not continue any edge type singularity of $u_0$ prominent at the boundary $\partial D$. To resolve this shortcoming the above mentioned TV-type inpainting models have been proposed. They are based on the functional $E_{\text{TV}}[u] = \frac{1}{2}\int_D |\nabla u| \, \mathrm{d}x$. Then the minimizing image intensity is a function of bounded variation; hence characterized by jumps along rectifiable edge contours. It solves - in a weak sense - the geometric PDE $h = 0$ where $h = \operatorname{div}(|\nabla u|^{-1} \nabla u)$ is the mean curvature on level sets or edge contours. Making use of the coarea formula (cf. [19]) one sees that minimizing $E_{\text{TV}}$ corresponds to minimizing the lengths of the level lines of $u$. Thus, the resulting edges will be straight lines.

In many applications the assumption of a sharp boundary $\partial D$ turns out to be a significant restriction. In fact, the reliability of the given image intensity gradually deteriorates from the outside to the inside of the inpainting region. This can be reflected by a relaxed formulation of the variational problem. In fact, one considers the functional

$$\mathcal{E}^\epsilon[u] = \int_\Omega |u - u_0|^2 \, H_\epsilon + \lambda(1 - H_\epsilon) \, |\nabla u|^p \, \mathrm{d}x \,,$$

where $\lambda > 0$, $p = 1$ or 2, and $H_\epsilon$ is a convoluted characteristic function $\chi_D$ and $\epsilon$ indicates the width of the convolution kernel [5]. In our case this blending function will depend on a confidence measure.

*Contribution.* In this paper, we address the restoration problem for locally corrupted optical flow fields. The underlying image information has not been exploited previously for optical flow restoration. We propose a novel anisotropic TV-type variational approach, where the anisotropy takes into account edge information of the underlying image sequence. To identify unreliable flow vectors, a confidence measure is used. This non binary measure can be taken into account as a weight in the functional. We validate our method on test data and on real world motion sequences with given ground truth.

## 2 The variational model

In this section we derive our restoration approach for optical flow fields. Given an image sequence, we denote by $u_0$ the image intensity and by $v_0$ the corresponding

estimated motion field at a fixed time $t$. Let us suppose that a confidence measure $\zeta$ is given together with a user selected threshold $\theta$, such that the set

$$[\zeta < \theta] := \{x \in \Omega \,:\, \zeta(x) < \theta\}$$

is the region of low confidence on the estimated optical flow field $v_0$. Hence, we aim at inpainting $v$ in the region $[\zeta < \theta]$.

*Design of an anisotropic prior.* Let us first construct the regularizing prior that is supposed to fill in the missing parts of the vector field. We choose the function $g(s) = (1 + \frac{s^2}{\mu^2})^{-1}$ (first proposed by Perona and Malik [20]) evaluated on the slope $\left|\nabla u_0^\delta\right|$ of the image intensity as an edge-sensitive weight. To ensure robustness, the intensity gradient is regularized via convolution with a Gaussian-type kernel $G_\delta(y) = \frac{1}{2\pi\delta}\exp(-\frac{y^2}{2\delta^2})$, i. e. $\nabla u_0^\delta = G_\delta * u_0$. In the spatially discrete model, we will realize this convolution via a single time step of the discrete heat equation (cf. Section 4). Thus, the weight $g(|\nabla u_0^\delta|)$ masks out edges of $u_0$.

In the vicinity of edges, we use a strongly anisotropic norm $\gamma(\nabla u_0^\delta, \mathcal{D}v)$ of the Jacobian $\mathcal{D}v$ of the motion field $v$ depending on the regularized gradient of the image intensity and defined as follows

$$\gamma(\nabla u_0^\delta, \mathcal{D}v) = \sqrt{\nu^2 \left|\mathcal{D}v\, n^\delta\right|^2 + \left|\mathcal{D}v\,(\mathbb{1} - n^\delta \otimes n^\delta)\right|^2}. \tag{1}$$

Here, $n^\delta = \frac{\nabla u_0^\delta}{|\nabla u_0^\delta|}$ is the regularized edge normal on the underlying image and $\mathbb{1}$ denotes the identity matrix of size 2. Furthermore, $x \otimes y{:=}(x_i y_j)_{i,j=1,2}$ is the usual definition of a rank one matrix which renders $\mathbb{1} - n^\delta \otimes n^\delta$ as the orthogonal projection on the direction orthogonal to the normal $n^\delta$. Hence, for a small parameter $\nu > 0$ and a point $x$ near a motion edge the value $\gamma(\nabla u_0^\delta(x), \mathcal{D}v(x))$ will be small if the motion edge is locally aligned with the underlying image edge and vice versa. In two space dimensions, one obtains

$$\left|\mathcal{D}v\,\left(\mathbb{1} - n^\delta \otimes n^\delta\right)\right|^2 = \sum_{i=1}^{2} \left((n^\delta)^\perp \cdot \nabla v_i\right)^2,$$

where $(n^\delta)^\perp = (n_2^\delta, -n_1^\delta)$. This easily follows for the unit length property $(n_1^\delta)^2 + (n_2^\delta)^2 = 1$ of the normal field $n^\delta$. Hence, the anisotropy $\gamma(\nabla u_0^\delta(x), \mathcal{D}v(x))$ simplifies to

$$\gamma(\nabla u_0^\delta, \mathcal{D}v) = \sqrt{\sum_{i=1}^{2} \left(\nu^2 \left(n^\delta \cdot \nabla v_i\right)^2 + \left((n^\delta)^\perp \cdot \nabla v_i\right)^2\right)}.$$

Finally, we obtain the following prior

$$\beta(\nabla u_0^\delta, \mathcal{D}v) = g(|\nabla u_0^\delta|)|\mathcal{D}v| + (1 - g(|\nabla u_0^\delta|))\gamma(\nabla u_0^\delta, \mathcal{D}v)\,. \tag{2}$$

Locally minimizing this prior will favor sharp motion edges aligned with edges in the underlying image. Apart from edges, a usual TV prior is applied to the

motion field. In particular, for larger destroyed regions this leads to an effective image based guidance in the reconstruction of motion edges. For $\nu$ values close to 1 there is no preference for any orientation of a motion edge and we obtain the classical TV-type inpainting model on motion fields.

Note that Nagel and Enkelmann [21] pioneered the idea of anisotropic image-driven smoothing in the context of optical flows and proposed an anisotropic prior that is closely related to the anisotropic part of $\beta$ (second part of (2)), while the isotropic part of $\beta$ (first part of (2)) was already proposed by Alvarez et al. [22]. In this regard, $\beta$ can be seen as an interpolation between existing isotropic and anisotropic priors. However, both [21] and [22] used their corresponding priors in the context of optical flow estimation, whereas we use the combined prior to inpaint the flow field in low confidence regions of the optical flow estimation.

*Dirichlet boundary conditions.* Based on the prior $\beta$, we can define the energy

$$\mathcal{E}_D[v] = \int_{[\zeta<\theta]} \beta(\nabla u_0^\delta(x), \mathcal{D}v(x))\,\mathrm{d}x \tag{3}$$

that has to be minimized on the set of functions $\mathcal{A} := \{v | v = v_0 \text{ on } \partial[\zeta < \theta]\}$. Note that with this model, it is crucial to choose the threshold $\theta$ conservatively to ensure the validity of the values of $v_0$ on $\partial[\zeta < \theta]$. If the chosen threshold is too low, the values used for the Dirichlet boundary conditions are possibly corrupted and may lead to undesirable inpainting results.

*Smooth overlapping blending.* Surely, the criterium to identify the inpainting domain, i.e. $[\zeta < \theta]$, is not sharp. Thus, we may select a parameter $\epsilon > 0$ for the width of the transition interval between full confidence and no confidence and define the blending function $x \to H_\epsilon(\mathrm{sdf}[\zeta - \theta](x))$, where $H_\epsilon(x) := \frac{1}{2} + \frac{1}{\pi}\arctan\left(\frac{x}{\epsilon}\right)$ (cf. the active contour approach by Chan and Vese [23]) and $\mathrm{sdf}[f]$ denotes the signed distance function of the set $[f < 0]$. Given this diffusive weight function, we can define the total energy

$$\begin{aligned}\mathcal{E}[v] = \int_\Omega \frac{1}{2}(v(x) - v_0(x))^2 H_\epsilon(\mathrm{sdf}[\zeta - \theta](x)) \\ + \lambda\,\beta(\nabla u_0^\delta(x), \mathcal{D}v(x))(1 - H_\epsilon(\mathrm{sdf}[\zeta - \theta](x) - \rho))\,\mathrm{d}x\,,\end{aligned} \tag{4}$$

which consists of two terms. The first term measures the distance from the precomputed motion field $v_0$ and acts as a relaxed penalty to ensure that $v \approx v_0$ in the region of confidence. The second term is a spatially inhomogeneous and anisotropic prior, primarily active on the complement of the confidence set. The parameter $\rho > 0$ leads to an overlap of the regions where the first and second term are active. If omitted, there are artifacts in the inpainting, cf. Figure 1.

## 3 First variation of the energy

As a core ingredient of the minimization algorithm we have to compute descent directions of the energy functional $\mathcal{E}[\cdot]$. Thus, let us derive explicit formulas

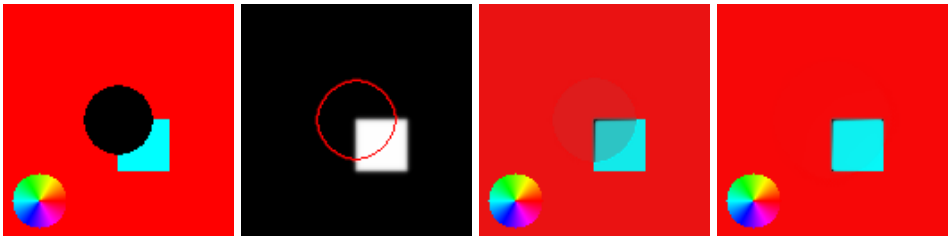

a) b) c) d)

**Fig. 1.** Effect of the overlapping of the fidelity and the regularity energy term (4), controlled by the parameter $\rho$. a) Corrupted flow field, b) Underlying image and corruption indicated by the red shape, c) Reconstructed flow field with $\rho = 0$, d) Reconstructed flow field with $\rho = 9h$.

for the variation of the different terms in the integrant of $\mathcal{E}$ with respect to $v$. We denote by $\langle \partial_w f, \vartheta \rangle$ a variation of a function $f$ with respect to a parameter function $w$ in a direction $\vartheta$. Using straightforward differentiation, for sufficiently smooth $v$, we obtain for $i \in \{1, 2\}$

$$\langle \partial_{v_i} \gamma(\nabla u_0^\delta, \mathcal{D}v), \vartheta \rangle = \frac{\left(\nu^2 (n^\delta \cdot \nabla v_i) n^\delta + \left((n^\delta)^\perp \cdot \nabla v_i\right)(n^\delta)^\perp\right) \nabla \vartheta}{\gamma(\nabla u_0^\delta, \mathcal{D}v)},$$

$$\begin{aligned}\langle \partial_{v_i} \beta(\nabla u_0^\delta, \mathcal{D}v), \vartheta \rangle = {} & g(|\nabla u_0^\delta|) \frac{\nabla v_i}{|\mathcal{D}v|} \cdot \nabla \vartheta + \\ & \frac{1 - g(|\nabla u_0^\delta|)}{\gamma(\nabla u_0^\delta, \mathcal{D}v)} \left(\nu^2 (n^\delta \cdot \nabla v_i) n^\delta + ((n^\delta)^\perp \cdot \nabla v_i)(n^\delta)^\perp\right) \cdot \nabla \vartheta \,.\end{aligned}$$

Finally, we derive the following variation $\langle \partial_{v_i} \mathcal{E}[v], \vartheta \rangle$ of the energy $\mathcal{E}[\cdot]$ with respect to the $i$-th component of the motion field $v$:

$$\begin{aligned}\langle \partial_{v_i} \mathcal{E}[v], \vartheta \rangle = \int_\Omega & H_\epsilon(\mathrm{sdf}[\zeta - \theta])(v_i - v_{i,0})\vartheta \\ & + \lambda(1 - H_\epsilon(\mathrm{sdf}[\zeta - \theta])) \Big[ g(|\nabla u_0^\delta|) \frac{\nabla v_i}{|\mathcal{D}v|} \cdot \nabla \vartheta + \\ & \frac{1 - g(|\nabla u_0^\delta|)}{\gamma(\nabla u_0^\delta, \mathcal{D}v)} \left(\nu^2 (n^\delta \cdot \nabla v_i) n^\delta + ((n^\delta)^\perp \cdot \nabla v_i)(n^\delta)^\perp\right) \cdot \nabla \vartheta \Big] \, \mathrm{d}x \,. \end{aligned} \tag{5}$$

The variation $\langle \partial_{v_i} \mathcal{E}_D[v], \vartheta \rangle$ is computed analogously.

## 4 The Algorithm

For the spatial discretization, we use the finite element (FE) method (cf. [24]): The whole domain $\Omega = [0, 1]^2$ is covered by a uniform quadrilateral mesh $\mathcal{C}$, on which a standard bilinear Lagrange finite element space is defined. We consider

the image $u_0$ and the components of the vector fields as sets of pixels, where each pixel corresponds to a node of the finite element mesh $\mathcal{C}$. Let $\mathcal{N} = \{x_1, ..., x_n\}$ denote the nodes of $\mathcal{C}$. The FE basis function of the node $x_i$ is defined as the continuous, piecewise bilinear function determined by $\varphi_i(x_i) = 1$ and $\varphi_i(x_j) = 0$ for $i \neq j$. To compute the integrals necessary to evaluate the energy $\mathcal{E}$ and its variations we employ a numerical Gauss quadrature scheme of order three (cf. [25]). All numerical calculations are done with double precision arithmetic.

As minimization method we use the following explicit gradient flow scheme with respect to a metric $g$. Initialize $v^0$ with the input vector field $v_0$ and iterate

$$v_j^{k+1} = v_j^k - \tau[\mathcal{E}, v^k, F[v^k]]G^{-1}F_j[v^k].$$

Here, $G$ denotes the matrix representation of the metric $g$ and the timestep width $\tau[\mathcal{E}, v^k, F[v^k]]$ is determined by the Armijo step size control [26] and depends by construction on the target functional $\mathcal{E}$, the current iterate of the solution $v^k$ and the descent direction $F[v^k]$. Let us emphasize that the choice of $g$ does not affect the energy landscape itself, but solely the descent path towards the set of minimizers.

The choice of the metric depends on the model used. In case of the smooth overlapping blending model (4), we chose $g$, inspired by the Sobolev active contour approach [27], to be a scaled version of the $H^1$ metric, i.e.

$$g(\vartheta_1, \vartheta_2) = \int_\Omega \vartheta_1 \cdot \vartheta_2 + \frac{\sigma^2}{2} \mathcal{D}\vartheta_1 : \mathcal{D}\vartheta_2 \, \mathrm{d}x$$

on variations $\vartheta_1, \vartheta_2$ of $v$ and where $\sigma$ represents a filter width of the corresponding time discrete and implicit heat equation filter kernel and $A : B = \mathrm{tr}(A^T B)$. The $i$-th component of the descent direction $F_j[v^k]$ is given by $(F_j[v^k])_i = \left\langle \partial_{v_j} \mathcal{E}[v], \varphi_i \right\rangle$.

In case of the Dirichlet boundary model (3), we choose $g$ as the Euclidean metric, i.e. $G = \mathbb{1}$ and the $i$-th component of the descent direction $F_j[v^k]$ is given by

$$(F_j[v^k])_i = \begin{cases} 0 & ; \, x_i \text{ Dirichlet node or } x_i \notin D, \\ \left\langle \partial_{v_j} \mathcal{E}_D[v], \varphi_i \right\rangle & ; \text{ else.} \end{cases}$$

Let us remark, that by construction of $F$ in the energy descent the Dirichlet boundary values are preserved. The step size control significantly speeds up the descent and at least experimentally ensures convergence.

The absolute value function is regularized by $|z|_\eta = \sqrt{z^2 + \eta^2}$ (here $\eta = 0.1$ is used). Alternatively to the gradient descent scheme the nonlinear Euler Lagrange equation could be solved iteratively by a freezing-coefficient technique [28]. The more sophisticated and very efficient method for Total Variation Minimization based on the dual formulation of the BV norm proposed by Chambolle [29] unfortunately cannot be applied to TV inpainting directly, because the weight of the fidelity term can vanish inside the inpainting domain.

## 5 Numerical Experiments and Applications

As already explained in the introduction, for applications such as motion compensation, motion segmentation or the computation of divergences in fluid dynamical flows, dense motion fields are required. To demonstrate the applicability of the presented approach for the inpainting of motion fields in regions indicated by a confidence measure we apply our method to artificial and real world data.

*Reconstruction of artificial motion fields.* As a first test case we consider the reconstruction of a corrupted rectangular and circular motion field. Figure 2 shows the color coded ground truth flow field on the left hand side (a), the red shape indicating the region to be reconstructed in the second image column (b), the corrupted input flow field that is also used as the initialization of the image guided motion inpainting algorithm in the third column (c), and the result of the algorithm on the right hand side (d). Obviously the method successfully retrieves the motion edge along the boundary of the square (first row) and the circle (second row). We used the following set of parameters: $\mu = 50$ and $\nu = 0.1$.

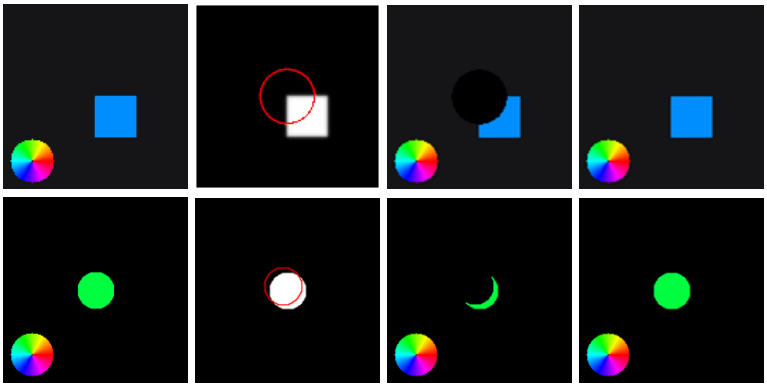

a) b) c) d)

**Fig. 2.** a) Ground truth flow field, b) Underlying image and corruption indicated by the red shape, c) Corrupted flow field which is the initialization of the image guided inpainting algorithm, d) Reconstruction result.

If the flow field to be inpainted not only contains destroyed regions, but is also corrupted by noise, enforcing Dirichlet boundary values on the boundary of the inpainting domain is not feasible. The blending model (4) on the other hand is well suited to handle such cases. In Figure 3 the motion edge is reconstructed along the boundary of the square present in the underlying image. Due to the nature of the regularization term, the reconstructed region does not contain any noise, while the noise is preserved in the complement of the inpainting domain. In between there is a smooth transition whose size is controlled by the regularization parameter of $H_\epsilon$. Note that the regularized region is bigger than

the inpainting domain because of the overlap induced by $\rho$. We used the following set of parameters: $\lambda = 0.01$, $\mu = 1$, $\nu = 0.1$.

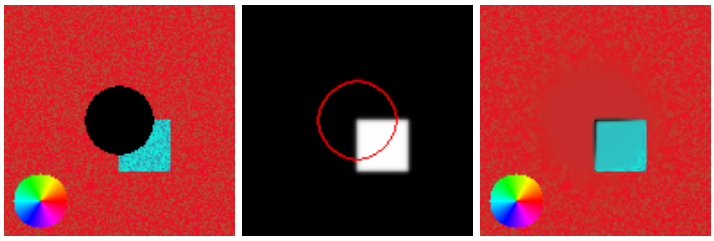

a) b) c)

**Fig. 3.** Results of the blending model (4) on noisy input data. a) Corrupted flow field, b) Underlying image and corruption indicated by the red shape, c) Reconstructed flow field with $\rho = 3h$.

*Reconstruction of real world motion fields.* Let us now consider real world examples and reconstruct the motion field of a sequence taken from the Middlebury dataset [30]. Special attention should be on the effect of the parameters $\mu$ and $\nu$ on the reconstruction result. Figure 4 shows the Rubber Whale sequence with corrupted regions indicated by a confidence measure and marked by red outlines (a), the ground truth flow field (b), the result of the image guided reconstruction algorithm (c) and the angular error (d). We used the following set of parameters: $\mu = 1$ and $\nu = 0.1$.

To investigate the effect of the parameter $\nu$ we take a closer look at two different regions in the scene: the upper left corner of the turning wheel on the left hand side and the flap of the box on the right hand side. At the upper boundary of the wheel the image contrast is low which renders the reconstruction along image edges difficult. Hence, the sensitivity of the method concerning the image gradient should be high and the method's inclination to follow image edges should be large as well, which would lead to a preference for small values $\mu$, $\nu$.

At the flap of the box the configuration is converse. The image contrast is large, but the motion edge does, in fact, not follow the stronger but the upper weaker edge. Hence the inclination of the method to follow image edges should be reduced, which would result in a higher value for $\nu$.

The effect of different parameter constellations for both regions is shown in Figure 5. The results demonstrate that for low $\nu$ values the wheel can be reconstructed quite well, but the motion field also follows the sharp edge of the box flap and yields errors in that part of the sequence. In contrast, for high $\nu$ values the box flap can be reconstructed well, but the wheel is reconstructed by a straight edge which does not follow its original contour.

*Comparison to diffusion and TV inpainting.* We compare the image guided motion inpainting algorithm to a linear diffusion and a TV inpainting method in

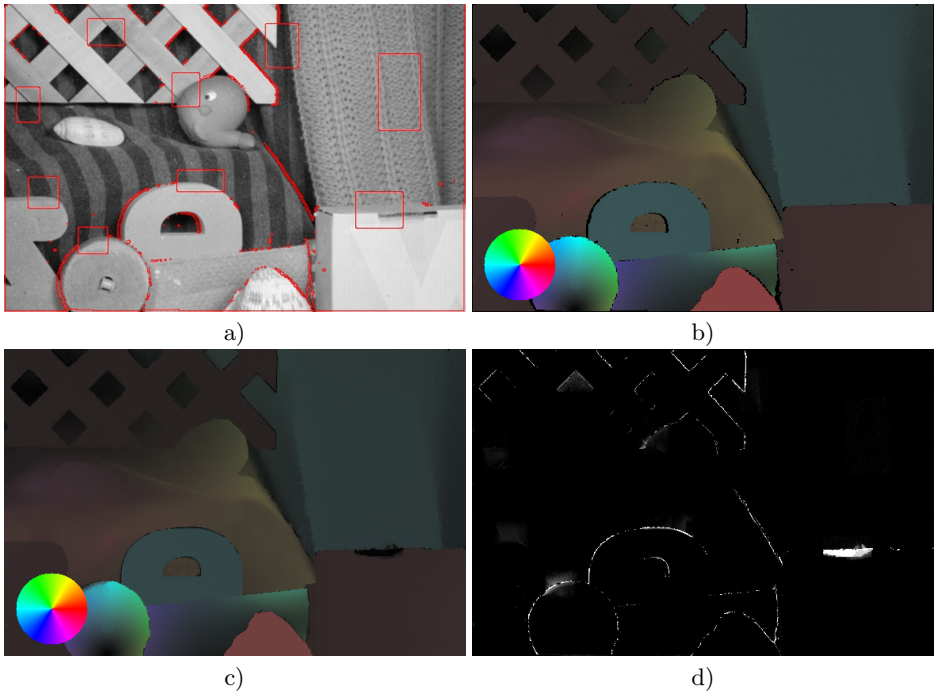


**Fig. 4.** a) Original Rubber Whale frame, b) Ground truth flow field, c) Reconstructed flow field, d) Resulting angular error.

case of the corrupted Marble sequence. Note that we confine the comparison to these relatively simple priors, because more sophisticated image driven priors like the one proposed by Nagel and Enkelmann [21] so far only have been used in the context of optical flow estimation but not for motion inpainting. Figure 6 shows the original corrupted sequence and the results of the diffusion based, the TV-based and the image guided motion inpainting methods. Not surprisingly, the diffusion based motion inpainting fails to reconstruct motion edges. In contrast, by means of TV motion inpainting flow edges can be reconstructed. However, the lower right corner of the central marble block cannot be reconstructed properly, because the exact course of the edges near the junction is unclear. Our image guided motion inpainting uses the image gradient information to correctly reconstruct the motion boundary of the central marble block as well. Here we used the following set of parameters: $\mu = 50$ and $\nu = 0.1$.

Finally, we consider a part of the Marble sequence that shows the junction mentioned before and apply artificial noise to the corrupted input. As noted earlier, using the Dirichlet boundary model is not feasible in such a case. Hence, the blending model (4) is used for the reconstruction. In Figure 7, the motion edge junction is properly reconstructed based on the information from the underlying image. We used the following set of parameters: $\lambda = 0.01$, $\mu = 1$, $\nu = 0.1$.

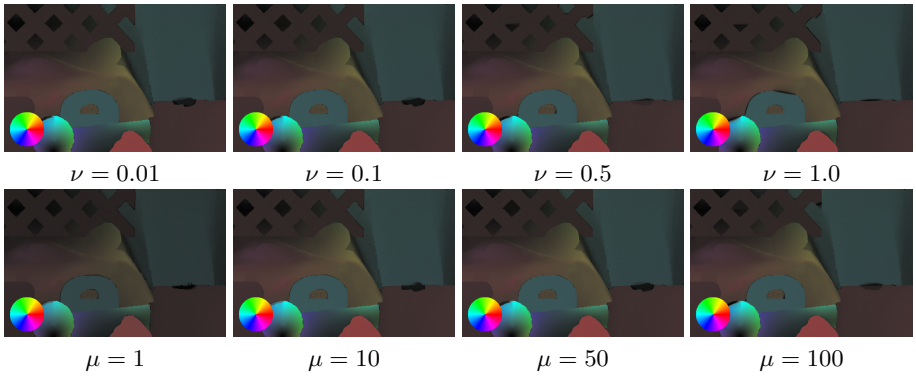


**Fig. 5.** Upper row: results for different values of $\nu$ for $\mu = 50$, lower row: results for different values of $\mu$ for $\nu = 0.1$.

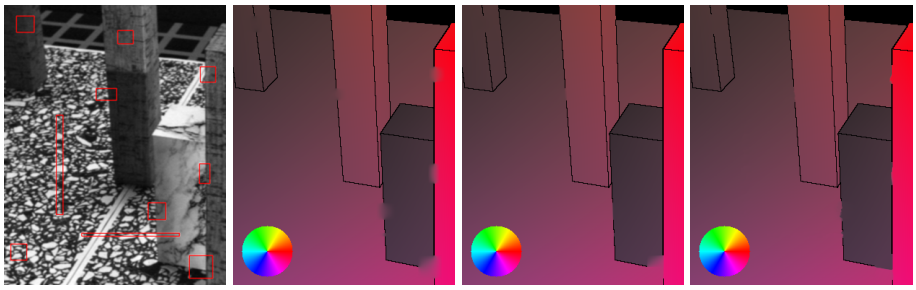


**Fig. 6.** Comparison of the proposed inpainting algorithm to diffusion and TV inpainting; the numbers indicate the average angular error within the corrupted regions after reconstruction; a) Original corrupted Marble sequence, b) Reconstruction result of diffusion based motion inpainting, c) Reconstruction result of TV based motion inpainting, d) Reconstruction result of image guided motion inpainting.

## 6 Conclusion and outlook

Given an image sequence and an extracted underlying motion field together with a local measure of confidence for the motion estimation, we have proposed a variational approach for the restoration of the motion field. This restoration is vital for a number of applications requiring dense motion fields. Based on a confidence measure, regions of corrupted motion can be detected. The underlying image data is still available and reliable. We make use of this information to improve the restoration of the motion field. The approach is based on an anisotropic TV-type functional, where the anisotropy takes into account edge information extracted from the underlying image data. The approach has been applied to test data and to two different real world optical flow problems. The results are compared to harmonic vector field inpainting and TV-type inpainting. We demonstrate that inpainting guided by the underlying intensity data outper-

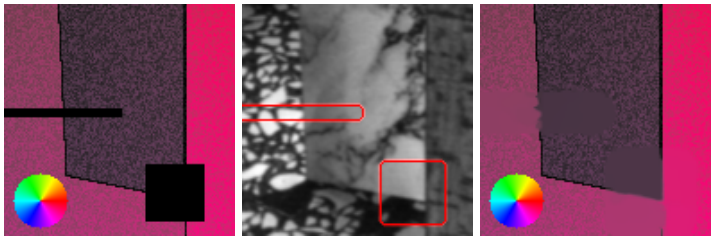

a) b) c)

**Fig. 7.** Results of the blending model (4) on noisy input data. a) Corrupted flow field, b) Underlying image and region of corrupted motion field indicated by the red shape, c) Reconstructed flow field with $\rho = 6h$.

forms purely flow driven approaches. We consider this as a feasibility study for the coupling of motion field and image sequence data in variational inpainting approaches. Robustness and reliability might be improved based on a fully joint approach, where the motion field and the image sequence are jointly restored. Furthermore, a restoration in space time would be promising as well.

Finally, a weakness of the proposed method is that for some motion fields the optimal performance is obtained in different locations for different parameter values (cf. Figure 5). To obtain the optimal performance in all locations, one should develop a methodology to locally adapt the parameters automatically after specifying a global set of parameters for the entire image.

## References


1. Bruhn, A., Weickert, J. In: A Confidence Measure for Variational Optic Flow Methods. Springer Netherlands (2006) 283–298
2. Kondermann, C., Kondermann, D., Jähne, B., Garbe, C.: An adaptive confidence measure for optical flows based on linear subspace projections. In: Pattern Recognition. Volume 4713 of LNCS., Springer (2007) 132–141
3. Kondermann, C., Mester, R., Garbe, C.: A statistical confidence measure for optical flows. In: Proceedings of the European Conference of Computer Vision, ECCV. (2008) 290–301
4. Masnou, S., Morel, J.: Level lines based disocclusion. In: Proceedings of the ICIP 1998. Volume 3. (1998) 259 – 263
5. Chan, T.F., Shen, J.: Mathematical models for local nontexture inpaintings. SIAM J. Appl. Math **62** (2001) 1019–1043
6. Chan, T.F., Shen, J.: Non-texture inpainting by curvature-driven diffusions. J. Visual Comm. Image Rep **12** (2001) 436–449
7. Telea, A.: An image inpainting technique based on the fast marching method. Journal of graphics tools **9**(1) (2003) 25–36
8. Bornemann, F., März, T.: Fast image inpainting based on coherence transport. Journal of Mathematical Imaging and Vision **28**(3) (2007) 259–278
9. Bertalmio, M., Bertozzi, A., Sapiro, G.: Navier-stokes, fluid dynamics, and image and video inpainting. In: IEEE Proceedings of the International Conference on Computer Vision and Pattern Recognition. Volume 1. (2001) 355–362

10. Chan, T., Shen, J.: Mathematical models for local non-texture inpaintings. SIAM J. Appl. Math. **62**(3) (2002) 1019–1043
11. Nitzberg, M., Mumford, D., Shiota, T.: Filtering, Segmentation and Depth (Lecture Notes in Computer Science Vol. 662). Springer-Verlag Berlin Heidelberg (1993)
12. Ballester, C., Bertalmio, M., Caselles, V., Sapiro, G., Verdera, J.: Filling-in by joint interpolation of vector fields and gray levels. IEEE Transactions on Image Processing **10**(8) (2001) 1200–1211
13. Ambrosio, L., Masnou, S.: A direct variational approach to a problem arising in image reconstruction. Interfaces and Free Boundaries **5** (2003) 63–81
14. Chan, T.F., Shen, J., Zhou, H.M.: Total variation wavelet inpainting. Journal of Mathematical Imaging and Vision **25**(1) (2006) 107–125
15. Patwardhan, K.A., Sapiro, G., Bertalmio, M.: Video inpainting of occluding and occluded objects. IMA Preprint Series 2016 (Januar 2005)
16. Matsushita, Y., Ofek, E., Weina, G., Tang, X., Shum, H.: Full-frame video stabilization with motion inpainting. IEEE Transactions on Pattern Analysis and Machine Intelligence **28**(7) (2006) 1150–1163
17. Chen, L., Chan, S., Shum, H.: A joint motion-image inpainting method for error concealment in video coding. In: IEEE International Conference on Image Processing (ICIP). (2006)
18. Kondermann, C., Kondermann, D., Garbe, C.: Postprocessing of optical flows via surface measures and motion inpainting. In: Pattern Recognition. Volume 5096 of LNCS., Springer (2008) 355–364
19. Ambrosio, L., Fusco, N., Pallara, D.: Functions of bounded variation and free discontinuity problems. Oxford Mathematical Monographs. Oxford University Press, New York (2000)
20. Perona, P., Malik, J.: Scale-space and edge detection using anisotropic diffusion. IEEE Transactions on Pattern Analysis and Machine Intelligence **12**(7) (July 1990) 629–639
21. Nagel, H.H., Enkelmann, W.: An investigation of smoothness constraints for the estimation of displacement vector fields from image sequences. IEEE Trans. Pattern Anal. Mach. Intell. **8**(5) (1986) 565–593
22. Alvarez, L., Monreal, L.J.E., Lefebure, M., Perez, J.S.: A pde model for computing the optical flow. In: Proc. XVI Congreso de Ecuaciones Diferenciales y Aplicaciones, Universidad de Las Palmas de Gran Canaria (September 1999) 1349–1356
23. Chan, T.F., Vese, L.A.: Active contours without edges. IEEE Transactions on Image Processing **10**(2) (2001) 266–277
24. Braess, D.: Finite Elemente. 2nd edn. Springer (1997) Theorie, schnelle Löser und Anwendungen in der Elastizitätstheorie.
25. Schaback, R., Werner, H.: Numerische Mathematik. 4te Aufl. edn. Springer-Verlag, Berlin (1992)
26. Kosmol, P.: Methoden zur numerischen Behandlung nichtlinearer Gleichungen und Optimierungsaufgaben. 2. edn. Teubner, Stuttgart (1993)
27. Sundaramoorthi, G., Yezzi, A., Mennucci, A.: Sobolev active contours. International Journal of Computer Vision. **73**(3) (2007) 345–366
28. Chan, T., Shen, J.: The role of the bv image model in image restoration. AMS Contemporary Mathematics (2002)
29. Chambolle, A.: An algorithm for total variation minimization and applications. Journal of Mathematical Imaging and Vision **20**(1-2) (November 2004) 89–97
30. Baker, S., Roth, S., Scharstein, D., Black, M., Lewis, J., Szeliski, R.: A database and evaluation methodology for optical flow. In: Proceedings of the International Conference on Computer Vision. (2007) 1–8